

SAR-U-Net: squeeze-and-excitation block and atrous spatial pyramid pooling based residual U-Net for automatic liver CT segmentation

Jinke Wang^{1,2}, Peiqing Lv², Haiying Wang², Changfa Shi^{3,*}

¹Rongcheng College, Harbin University of Science and Technology, Rongcheng, 264300, China

²School of Automation, Harbin University of Science and Technology, Harbin, 150080, China

³Mobile E-business Collaborative Innovation Center of Hunan Province, Hunan University of Technology and Business, Changsha, 410205, China

Abstract

Background and objective: Liver segmentation is an essential prerequisite for liver cancer diagnosis and surgical planning. Traditionally, liver contour is delineated manually by radiologist in a slice-by-slice fashion. However, this process is time-consuming and prone to errors depending on radiologist's experience. In this paper, a modified U-Net based framework is presented, which leverages techniques from Squeeze-and-Excitation (SE) block, Atrous Spatial Pyramid Pooling (ASPP) and residual learning for accurate and robust liver CT segmentation, and the effectiveness of the proposed method was tested on two public datasets LiTS17 and SLiver07.

Methods: A new network architecture called SAR-U-Net was designed, which grounded in the classic U-Net. Firstly, the SE block is introduced to adaptively extract image features after each convolution in the U-Net encoder, while suppressing irrelevant regions, and highlighting features of specific segmentation task; Secondly, ASPP was employed to replace the transition layer and the output layer, and acquire multi-scale image information via different receptive fields. Thirdly, to alleviate the degradation problem, the traditional convolution block was replaced with the residual block and thus prompt the network to gain accuracy from considerably increased depth.

Results: In the LiTS17 database experiment, the mean values of *Dice*, *VOE*, *RVD*, *ASD* and *MSD* were 95.71 ± 0.55 , 9.52 ± 1.11 , -0.84 ± 3.86 , 1.54 ± 0.30 and 29.14 ± 2.63 , respectively. Compared with other closely related 2D-based models, the proposed method achieved the highest accuracy. In addition, in the experiment of the SLiver07 dataset, the mean values of *Dice*, *VOE*, *RVD*, *ASD* and *MSD* were 97.31 ± 1.49 , 5.37 ± 3.27 , -1.08 ± 2.06 , 1.85 ± 0.30 and 27.45 ± 1.89 , respectively. Compared with other closely related models, the proposed method achieved the highest segmentation accuracy except for the *RVD*.

Conclusion: An improved U-Net network combining SE, ASPP, and residual techniques is developed for automatic liver segmentation from CT. This new model enables a great improvement on the accuracy compared to 2D-based models, and its robustness in circumvent challenging problems, such as small liver regions, discontinuous liver regions, and fuzzy liver boundaries, is also well demonstrated and

*Corresponding author: ivanhanks@gmail.com

validated.

Keywords: Liver Segmentation, CT, U-Net, Squeeze-and-Excitation, Atrous Spatial Pyramid Pooling, Residual

1 Introduction

Liver segmentation is a key prerequisite for cancer detection and treatment. In order to acquire accurate information on the liver volume, position and shape from abdominal CT, radiologist needs to manually label slices one by one. However, this process is labor-intensive and is also subject to the radiologist's experience (**Figure 1** shows three challenging cases). Therefore, there is an urgent clinical need for automatic and accurate liver segmentation methods.

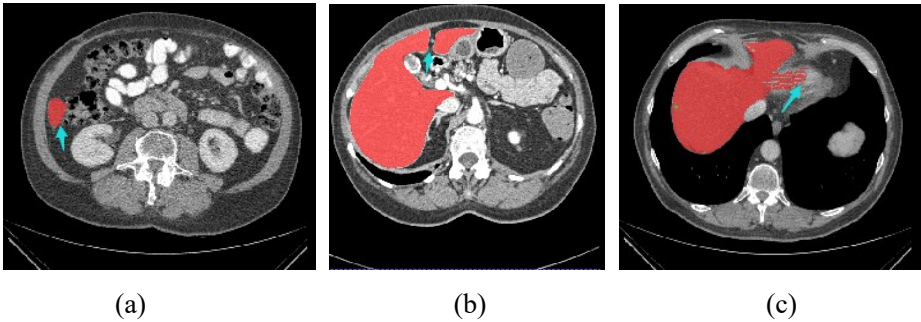


Figure 1. Challenging cases (a) Small liver area (b) Discontinuity liver area (c) Blurred liver boundary.

In the past few decades, many sophisticated strategies have been developed by researchers for automatic liver segmentation, which can be roughly divided into three categories, which are intensity-based methods [1-5], machine learning-based methods [6-11], and deep learning-based methods [12-22].

For the intensity-based approach, it is known for fast speed, including thresholding-based methods [1-2], region growing method [3] and level set method [4-5]. However, most of them are semi-automatic approaches, which are susceptible to noise, and require human intervention with complicated parameter setting.

For machine learning-based approach, it enables a great improvement on the segmentation accuracy [6-11]. However, most machine learning-based approaches require manual design of specific features, which makes a great impact on the accuracy. On the contrary, deep learning-based methods, such as convolutional neural networks (CNN), have developed rapidly due to their intelligent processing of feature engineering, and have achieved a series of successes in tasks such as target detection, image segmentation and classification [12-14].

Among deep learning-based methods, Fully Convolutional Networks (FCN) has attracted much attention due to its remarkable pixel-level classification. This model was first proposed by Long et al. [15], and its main difference from CNN is that the fully connected layers of CNN are replaced with the convolutional layers. Ronneberger et al. [16] proposed the U-Net model on the basis of FCN, which has achieved great success in the field of medical image segmentation and has inspired many scholars to participate in the improvement of U-Net model. Milletar et al. [17] proposed V-Net, in which

residual learning mechanism [18] was combined with U-Net to directly achieve end-to-end segmentation on 3D medical images. Christ et al. [19] suggested a method of cascading two FCNs to segment the regions of liver and tumor, respectively, and employed 3D Conditional Random Field (CRF) to optimize the segmentation results. Kaluva et al. [20] tried putting dense modules into FCN, and obtained good results in liver and tumors segmentations. Li et al. [21] developed the H-Dense U-Net model, which combines 2D U-Net and 3D U-Net models to make full use of the information in and between slices for higher tumor segmentation accuracy, and meanwhile, greatly alleviates the problem of high memory consumption caused by single 3D training method. Han et al. [22] designed a 24-layer FCN model, in which a skip connection is used between encoder and decoder modules, to achieve the purpose of merging low-level details and high-level semantic information.

The traditional U-Net based method is quite successful in medical image classification. However, there are still some shortcomings. First of all, the feature map after U-Net convolution lacks a targeted refining process of feature information. Second, the problem of category imbalance could easily lead to errors on small liver regions, discontinuous liver regions and blurred liver boundaries; Moreover, the process of gradual down-sampling of the U-Net network could reduce the resolution of the image, resulting in a decrease in segmentation accuracy. Finally, with the deepening of the network depth, it is easy to induce the degradation problems.

2 Related Works

We briefly review the most related works, including attention mechanism, atrous convolution and residual learning.

2.1 Attention mechanism

In recent years, the framework of attention-based image classification and segmentation have achieved great successes in the field of computer vision [23-24]. The attention-based network can not only focus on specific tasks, but also suppress irrelevant areas. According to whether it is differentiable, it could be divided into hard attention and soft attention [25-26]. For hard attention, the gradient can be calculated by the neural network, while the weight of attention could be learned via forward propagation and backward feedback [26]. Hu et al. [27] proposed an attention module named SE block, which automatically obtains the weight of each feature channel, and won the ImageNet2017 competition in image classification task. Noori et al. [36] successfully applied the SE Block to the automatic segmentation of brain tumors, as the feature map of the U-Net encoder and the corresponding feature map of the decoder were joined, the SE Block was embedded into it to obtain proper attention weight. Compared with the hard attention mechanism, the soft attention is considered as a global weight calculation approach. Oktay et al. [28] developed an attention gate (AG) before splicing the image features obtained by the encoder convolution with the corresponding features in the decoder, and readjusted the output features of the encoder, which was successfully applied to pancreas segmentation in CT. Schlemper et al. [29] presented a soft attention mechanism to generate a gated signal that can be trained end-

to-end, and effectively validated in fetal ultrasound screening.

2.2 Atrous convolution

The atrous convolution was first proposed by Yu et al. [32], which adds holes (dilations) to the standard convolution to increase the receptive field. It can effectively alleviate the problem of reduced spatial resolution caused by down-sampling. Therefore, atrous convolution is widely used in the field of image segmentation. Chen et al. [34] applied the atrous convolution to the deep CNNs model and provided the novel DeepLab V1 model, to obtain more context information. Chen et al. [30] made further improvements to the dilated convolution and proposed the ASPP module. For a given input, ASPP can sample the atrous convolution with different sampling rates, which is equivalent to capturing the context of the image at multiple scales. It enables the obtained feature map to contain richer semantic information, which is also crucial for accuracy.

2.3 Residual learning

The residual structure was first proposed by He et al. [18]. This model could solve the degradation problem while the network depth increases. Jin et al. [34] provided a 3D hybrid residual attention-aware segmentation method, which embed residual structure into the basic U-Net, and confirmed a success in liver and tumors segmentations. Bi et al. [35] suggested a deep residual network (ResNet) for effective liver lesions segmentation, and ranked the 4th in the LiTS2017 liver segmentation challenge.

The aforementioned methods work well for most automatic liver segmentation situations. However, when it is directly applied to the clinic, its accuracy and robustness are still insufficient, which heavily hampers the further application of U-Net model. To overcome the shortcomings of traditional U-Net in the automatic liver segmentation is exactly what we concern in this paper. Here, we leverage the abovementioned three sophisticated techniques, and present an innovative end-to-end automatic segmentation framework, which is called SAR-U-Net¹, with the main contributions of this paper as follows:

- (1) Follow the convolution of the encoder in U-Net, the attention mechanism is introduced, so that it can derive image features in an adaptive manner, and meanwhile, suppress irrelevant areas, thus ensure the network could focus on the features related to the specific segmentation task.
- (2) Replace the transition layer and the final output layer of the U-Net decoder with ASPP, so as to achieve the purpose of extracting richer multi-scale feature information.
- (3) Replace the standard convolutional layer of U-Net with the residual block, and attach a batch normalization layer, which promotes faster convergence, eliminates vanishing gradient problem, and improves segmentation accuracy by training deeper networks.

The whole paper is arranged as follows, Section 3 provides a detailed description

¹ Our code is publicly available at <https://github.com/lvpeiying/SAR-U-Net-liver-segmentation>.

of the proposed SAR-U-Net structure, loss function and evaluation metrics, and Section 4 shows the experiments and quantitative comparisons. The last section gives the conclusion of this paper.

3 Method

3.1 SAR-U-Net Architecture

The proposed network SAR-U-Net is composed of two parts forming a symmetrical structure: the encoder and the decoder part (**Figure 2**). The encoder is responsible for feature extraction, while the decoder is responsible for feature positioning. The whole architecture consists of 8 residual blocks, 4 pooling layers, 4 SE (Squeeze and Excitation Block), 2 ASPP and multiple up-sampling blocks. The size of convolution kernel is 3×3 , the pooling layer size is 2×2 , and the input image is $512 \times 512 \times 1$. As each feature image passed through a series of operations such as convolution, feature extraction and pooling, and then the binary segmented image of 512×512 is obtained.

In the entire network, the ordinary unit of the traditional U-Net is replaced by the residual learning structure [18]. Comparatively, the residual structure adds shortcut connections on the basis of a single forward propagation, so that a deeper network can be trained without degradation, while extracting more discriminative features. In the residual unit, batch normalization and ReLU activation operations are performed following each convolution. For the introduction of batch normalization, it can not only reduce the sensitivity of the model to the initialization parameters, but also exerts the regularization effect to a certain extent. For the ReLU function, it is most widely used for activation thanks to its effective ability of circumvent the vanishing gradient problem.

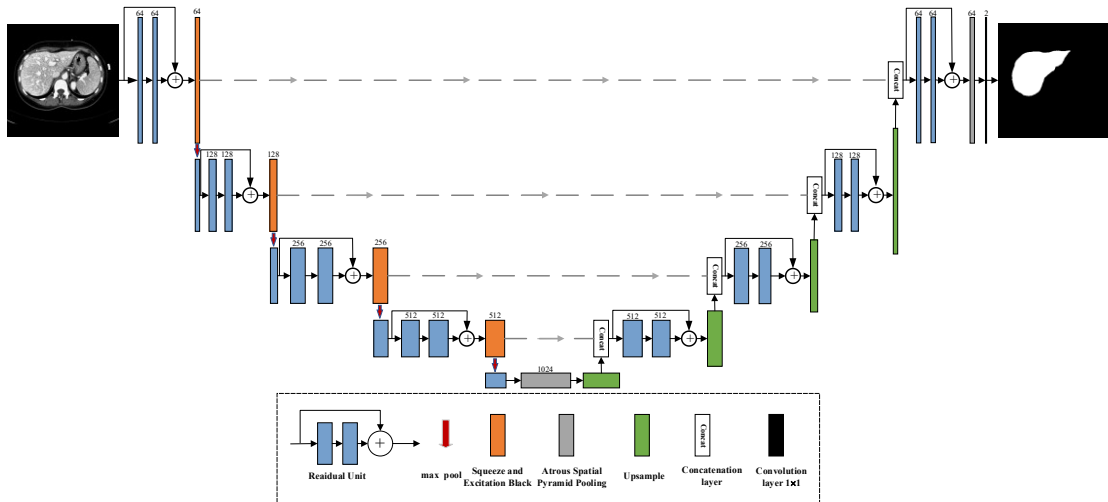


Figure 2. Architecture of proposed SAR-U-Net

In addition, to derive information from the feature map of encoder convolution, SE block [27] is utilized after each residual unit, to adaptively extract the image features. Thus, thanks to the channel attention mechanism, the network is enabled to focus on

the specific segmentation task (as shown in **Figure 3**).

The specific operation of the SE module is as follows: First, the 2D feature ($H \times W$) of each channel is compressed into a real number by global average pooling, and then, using a fully connected neural network, a nonlinear transformation is performed to obtain the weight of each feature channel, and finally, the normalized weights obtained above are weighted to the features of each channel, so as to achieve the purpose of extracting specific information.

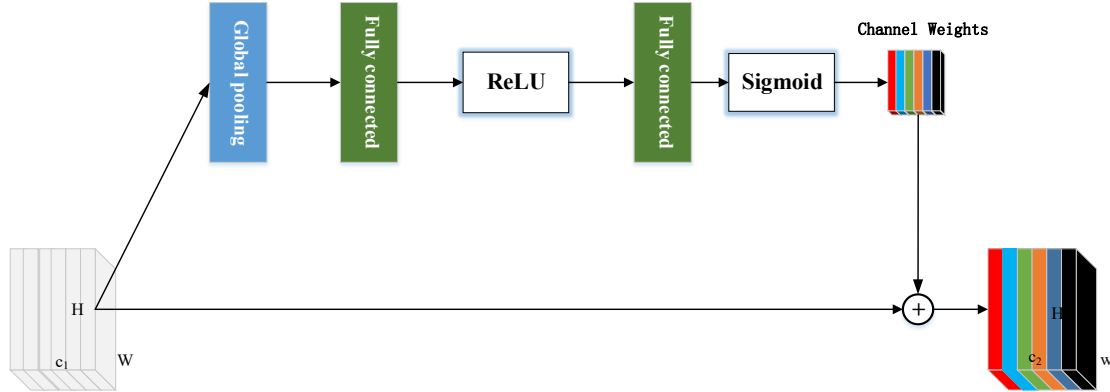


Figure 3. Squeeze and Excitation Block

Furthermore, to alleviate the problem of resolution degradation caused by multiple down-sampling, ASPP [30] is utilized as the transition layer of the network (as shown in **Figure 4**). The ASPP module is able to capture the contextual information of the image at multiple scales, which promotes the inclusion of multi-scale semantic information in the extracted feature map. Similarly, the ASPP module is also introduced in the output of the decoder part, by which way, the accuracy is increased together with the transition layer.

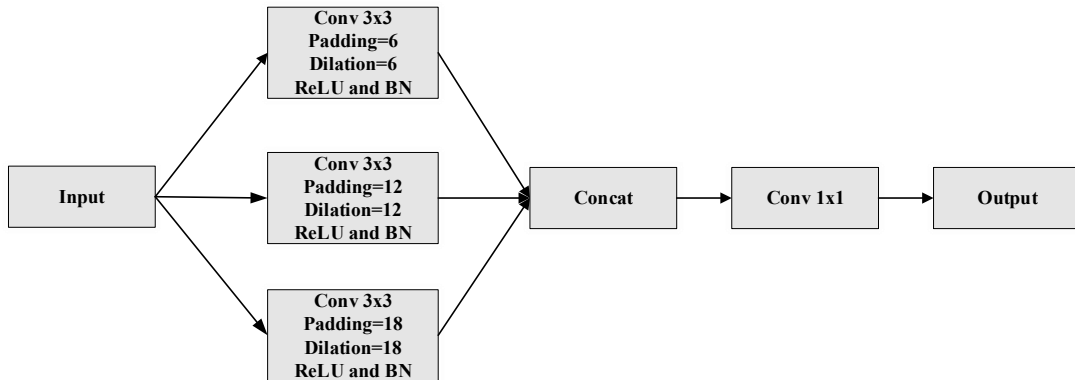


Figure 4. Atrous Spatial Pyramid Pooling

The detailed structure of the proposed network is listed in **Table 1**. The 2nd and 5th columns indicate the size and channels of the output. For the 3rd and 6th columns, $[\]$ denotes the convolution operation, while " $3 \times 3, 64$ " denotes the convolution kernel of size 3×3 and convolution layer of 64 channels. In addition, the "+" in

"Upsample_1+SE_Black4" represents a connection between Upsample_1 and SE_Black4, which results in Concatenate1. Moreover, The "→" in the 3rd column denotes the operation sequence.

Table 1. SAR-U-Net Network Constructure

	Feature size	2D SAR-U-Net		Feature size	2D SAR-U-Net
Input	512×512×1		Upsample_1	64×64×1024	2×2
Conv1_x	512×512×64 512×512×64	$\begin{bmatrix} 3 \times 3, 64, \text{BN-ReLU} \\ 3 \times 3, 64, \text{BN-ReLU} \end{bmatrix}$	Concatenate1	64×64×1536	Upsampe_1+SE_Block 4
SE_Block1	512×512×64	Avg_pool(1,1)→Linear(64,4) →ReLU→Linear(4,16) → Sigmoid	Conv5_x	64×64×512	$\begin{bmatrix} 3 \times 3, 512, \text{BN-ReLU} \\ 3 \times 3, 512, \text{BN-ReLU} \end{bmatrix}$
Maxpooling	256×256×64	2×2	Upsample_2	128×128×512	2×2
Conv2_x	256×256×128 256×256×128	$\begin{bmatrix} 3 \times 3, 128, \text{BN-ReLU} \\ 3 \times 3, 128, \text{BN-ReLU} \end{bmatrix}$	Concatenate2	128×128×756	Upsample_2+ SE_Block3
SE_Block2	256×256×128	Avg_pool(1,1)→Linear(128,8) →ReLU→Linear(8,128) → Sigmoid	Conv6_x	128×128×256	$\begin{bmatrix} 3 \times 3, 256, \text{BN-ReLU} \\ 3 \times 3, 256, \text{BN-ReLU} \end{bmatrix}$
Maxpooling	128×128×128	2×2	Upsample_3	256×256×256	2×2
Conv3_x	128×128×256 128×128×256	$\begin{bmatrix} 3 \times 3, 256, \text{BN-ReLU} \\ 3 \times 3, 256, \text{BN-ReLU} \end{bmatrix}$	Concatenate3	256×256×384	Upsample_3+ SE_Block2
SE_Block3	128×128×256	Avg_pool(1,1)→Linear(256,16) →ReLU→Linear(16,256) → Sigmoid	Conv7_x	256×256×128	$\begin{bmatrix} 3 \times 3, 128, \text{BN-ReLU} \\ 3 \times 3, 128, \text{BN-ReLU} \end{bmatrix}$
Maxpooling	64×64×256	2×2	Upsample_4	512×512×128	2×2
Conv4_x	64×64×512 64×64×512	$\begin{bmatrix} 3 \times 3, 512, \text{BN-ReLU} \\ 3 \times 3, 512, \text{BN-ReLU} \end{bmatrix}$	Concatenate4	512×512×192	Upsample_4+SE_Bloc k1
SE_Block4	64×64×512	Avg_pool(1,1)→Linear(512,32) →ReLU→Linear(32,612) → Sigmoid	Conv8_x	512×512×64	$\begin{bmatrix} 3 \times 3, 64, \text{BN-ReLU} \\ 3 \times 3, 64, \text{BN-ReLU} \end{bmatrix}$
Maxpooling	32×32×512	2×2	ASPP2	512×512×64	
ASPP1	32×32×1024		Conv9_x	512×512×2	$[1 \times 1, 1]$

3.2 Loss function

Cross entropy is widely used in various model training by measuring the similarity between the predicted distribution and the ground truth, with its formula as follows,

$$L = -\frac{1}{N} \sum_{i=1}^N [\hat{P}_i \log P_i + (1 - \hat{P}_i) \log (1 - P_i)] \quad (1)$$

in which, P_i represents the probability that voxel i belongs to the foreground, while \hat{P}_i represents the gold standard, and N denotes the number of samples.

However, in the actual liver segmentation, due to the unbalanced ratio of foreground (liver) and background (non-liver), it is likely to cause missed segmentation

of small liver regions. Therefore, the following balancing operations are performed, in which an additional weight factor ω_i^{class} is introduced to weight the loss function in the original **Equation (1)**, with the formular as follows,

$$L = -\frac{1}{N} \sum_{i=1}^N \omega_i^{class} [\hat{P}_i \log P_i + (1 - \hat{P}_i) \log (1 - P_i)] \quad (2)$$

$$\omega_i^{class} = \frac{N - n_i}{n_i} \quad (3)$$

where n_i presents the number of pixels belonging to class i .

3.3 Evaluation Metrics

For liver segmentation evaluation, five most commonly used metrics are adopted, including *Dice* coefficient, Volume Overlap Error (*VOE*), Relative Volume Error (*RVD*), Average Symmetric Surface Distance (*ASD*) and Maximum Surface Distance (*MSD*). Assuming that, A is the segmentation result of the liver, and B is the ground truth, then the definitions of the five metrics are as follows:

(1) *Dice*: the similarity of two sets, whose range is $[0,1]$. The larger the value, the higher the segmentation accuracy.

$$Dice(A, B) = \frac{2|A \cap B|}{|A| + |B|} \quad (4)$$

(2) *Volume Overlap Error (VOE)*: the difference between the segmented volume and the ground truth volume.

$$VOE(A, B) = 1 - \frac{|A \cap B|}{|A \cup B|} \quad (5)$$

(3) *Relative Volume Error (RVD)*: Used to determine whether the segmentation result is over-segmented or under-segmented. The closer the value is to zero, the higher accuracy of the segmentation.

$$RVD(A, B) = \frac{|B| - |A|}{|A|} \quad (6)$$

(4) *Average Symmetric Surface Distance (ASD)*: the average distance between the surfaces of segmentation results A and the ground truth B , where $d(v, S(X))$ represents the shortest Euler distance from voxel v to the surface voxel of the segmentation result.

$$ASD(A, B) = \frac{1}{|S(A)| + |S(B)|} \left(\sum_{p \in S(A)} d(p, S(B)) + \sum_{q \in S(B)} d(q, S(A)) \right) \quad (7)$$

(5) *Maximum Surface Distance (MSD)*: the maximum surface distance between the segmentation results A and the ground truth B .

$$MSD(A, B) = \max \left\{ \max_{p \in S(A)} d(p, S(B)), \max_{q \in S(B)} d(q, S(A)) \right\} \quad (8)$$

4. Experiment

4.1 Dataset and implementation

In the experiment, the labeled training sets of the LiTS17² and SLiver07³ datasets are used. The LiTS17-Training dataset consists of 131 sets of 3D abdominal CT scans, with a variety of different sampling protocols. The size of each CT image and labels is 512×512 , and the in-plane resolution is $0.55\text{mm} \sim 1.0\text{mm}$, with the inter-slice spacing $0.45\text{mm} \sim 6.0\text{mm}$. In our experiment, 121 datasets were randomly selected from the 131-training set for training, while the other 10 datasets are used for testing. In addition, the SLiver07-Training dataset consists of 20 sets of datasets, in which the size of each CT image is 512×512 , and the in-plane resolution is $0.56\text{mm} \sim 0.8\text{mm}$, with the inter-slice spacing $1\text{mm} \sim 3\text{mm}$, and all the 20 datasets were used for testing.

In the training phase, the initial value of the learning rate (lr) is set to 0.001, and is attenuated according to the formula $lr = initial_lr \times \gamma^{epoch/step_size}$, where the initial value ($initial_lr$) is set to 0.5, and the $step_size$ is set to 4. We use standard SGD (Stochastic Gradient Descent) to optimize the objective function. The $batch$ size is set to 4, and the total $epoch$ is set to 60. All the experiments are run on a workstation with Ubuntu 18.04 operating system, graphics card RTX2080Ti, memory 64G, single CPU Intel Xeon Silver 4110, and using the Pytorch1.4 deep learning framework for implementation.

4.2 Image preprocessing

In the preprocessing stage, first, to remove irrelevant organs, the Hounsfield intensity is transformed to $[-200, 200]$, and histogram equalization is applied to enhance the contrast and clarity of the image (as shown in **Figure 5(b)**). Then, the z-axis spacing of all data is resampled to 1mm, and the intensity of the image is normalized to $[0,1]$ (as shown in **Figure 5(c)**). Finally, in order to further optimize the model weight during training, all the pixel values are standardized.

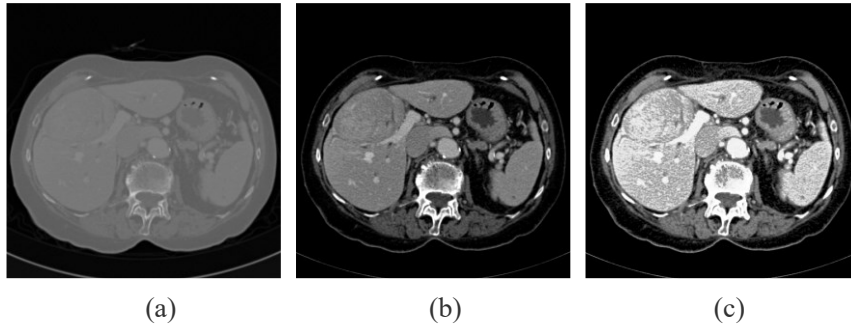


Figure 5. Flowchart of preprocessing. (a) Original CT (b) HU window processing (c) Histogram equalization

4.3 Dataset augment

To eliminate the overfitting problem in the training process, data augment is an alternative strategy via expanding the training datasets. In this step, a variety of rigid and elastic transformations were utilized, including: (1) scaling the image between 0.8 and 1.2 with a 50% probability (**Figure 6(b-c)**), (2) rotating the image between 0 degrees and 30 degrees with a 30% probability (**Figure 6(d)**), (3) turning the image left-right or up-down with a 30% probability (**Figure 6(e)**), and (4) B-spline elastic

² <https://competitions.codalab.org/competitions/17094#results>

³ <http://www.sliver07.org/>

deformation [31] (Figure 6(f)).

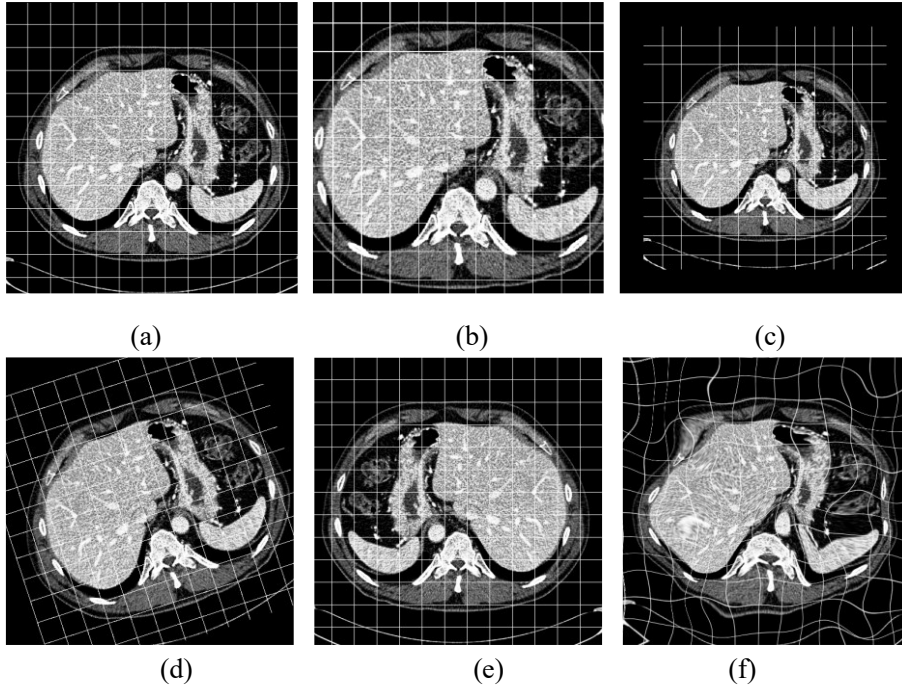


Figure 6. Data augment. (a) Original CT (b) Zoom in (c) Zoom out (d) Rotation (e) Rolling over (f) Elastic deformation

4.4 Test on LiTS17-Training dataset

The proposed method is compared with 3 related classic models, including the FCN⁴ model based on the VGGNet framework [15], U-Net⁵ [16] and Attention U-Net⁶ [28]. To ensure a fair comparison and reproductivity of the experiment, the open-source codes of the above models were provided and used for training and testing with the same datasets, respectively. The input of all training models is 2D image, while the lesion label and the liver label are merged for liver training purpose.

4.4.1 Quantitative analysis of segmentation accuracy

Table 2 shows the quantitative comparison results of the four models. It can be seen from **Table 2** that, our proposed model showed significant advantages in the comparisons on five evaluation metrics, especially for the *Dice*, our method obtains the highest accuracy of 95.71 ± 0.55 . Compared with the other three models, the FCN model shows low performances in *Dice*, *VOE*, *RVD* and *MSD*, which results in a biggest gap with the ground truth. Compared with U-Net and Attention U-Net, the *Dice* and *MSD* of our proposed model have greatly improved, while *VOE*, *RVD* and *ASD* metrics are also slightly improved. A detailed performance of the proposed model with the LiTS17 datasets is also provided in **Table 3**.

In the comparative experiment, the statistical method *t*-test is also used to verify whether the proposed method is significantly different from other methods on the

⁴ <https://github.com/shelhamer/fcn.berkeleyvision.org>

⁵ <https://github.com/milesial/Pytorch-U-Net>

⁶ <https://github.com/ozan-oktay/Attention-Gated-Networks>

accuracy. All statistical hypothesis tests are based on the representative metrics of *Dice* and *ASD*. As shown in **Table 2**, the performance difference between the labeled results and our proposed results is statistically significant ($p < 0.05$).

Table 2 Quantitative results among the four methods on 10 Lits17-Training datasets

Methods	Dice (%)	VOE (%)	RVD (%)	ASD (mm)	MSD (mm)
FCN[15]	88.63±4.28*	20.15±6.84	-15.57±9.28	3.46±1.05*	38.23±3.29
U-Net[16]	92.60±2.54*	10.33±1.69	-0.28±6.13	2.41±0.54*	33.69±1.89
Attention U-Net[28]	94.71±0.72*	10.25±1.30	-1.69±3.13	2.45±0.46*	30.25±2.62
Ours	95.71±0.55	9.52±1.11	-0.84±3.86	1.54±0.30	29.14±2.63

Results are represented as mean and standard deviation. Note: * indicates a statistically significant difference between the marked result and the corresponding one of our method at a significance level of 0:05.

Table 3 The results of our proposed method on 10 Lits17-Training datasets

Case Num	Dice	VOE	RVD	ASD (mm)	MSD (mm)
1	0.955	0.103	-0.029	1.568	28.453
2	0.963	0.089	-0.033	1.471	34.951
3	0.956	0.100	-0.049	1.382	31.259
4	0.968	0.097	-0.048	1.494	25.494
5	0.949	0.114	-0.040	1.797	28.315
6	0.953	0.107	-0.038	1.933	29.756
7	0.960	0.094	0.034	1.229	30.657
8	0.961	0.073	0.043	0.955	39.421
9	0.954	0.086	0.036	1.673	34.598
10	0.952	0.090	0.040	1.863	28.534
Avg	0.957	0.095	-0.0084	1.544	29.144

4.4.2 Visual segmentation results on challenging liver cases

Figure 7 provides typical segmentation comparisons between the proposed method and other 3 classic algorithms when handling challenging problems. The first and second rows in **Figure 7** show the comparison results of the small liver area. It can be seen that, all the models are able to segment the liver area properly, except for partial over-segmentation or under-segmentation that occur in FCN, U-Net and Attention U-Net models. In contrast, our proposed model successfully circumvents such errors.

In addition, the third and fourth rows of images in **Figure 7** show the comparison results of discontinuous regions of the liver. It can be seen that, the FCN model performs the worst. The FCN model not only misses the liver area, but also leads to typical under-segmentation errors. Although U-Net, Attention U-Net and our proposed models shows significant advantages when dealing with organs adjacent to the liver, some under-segmentation still occurred.

Furthermore, the fifth and sixth rows of **Figure 7** show the comparison results with blurred liver boundaries. It can be seen that, FCN and U-Net perform relatively poorly, with typical over- and under-segmentation errors. However, thanks to the attention mechanism, Attention U-Net showed a slight under-segmentation error, and our model successfully avoided the error.

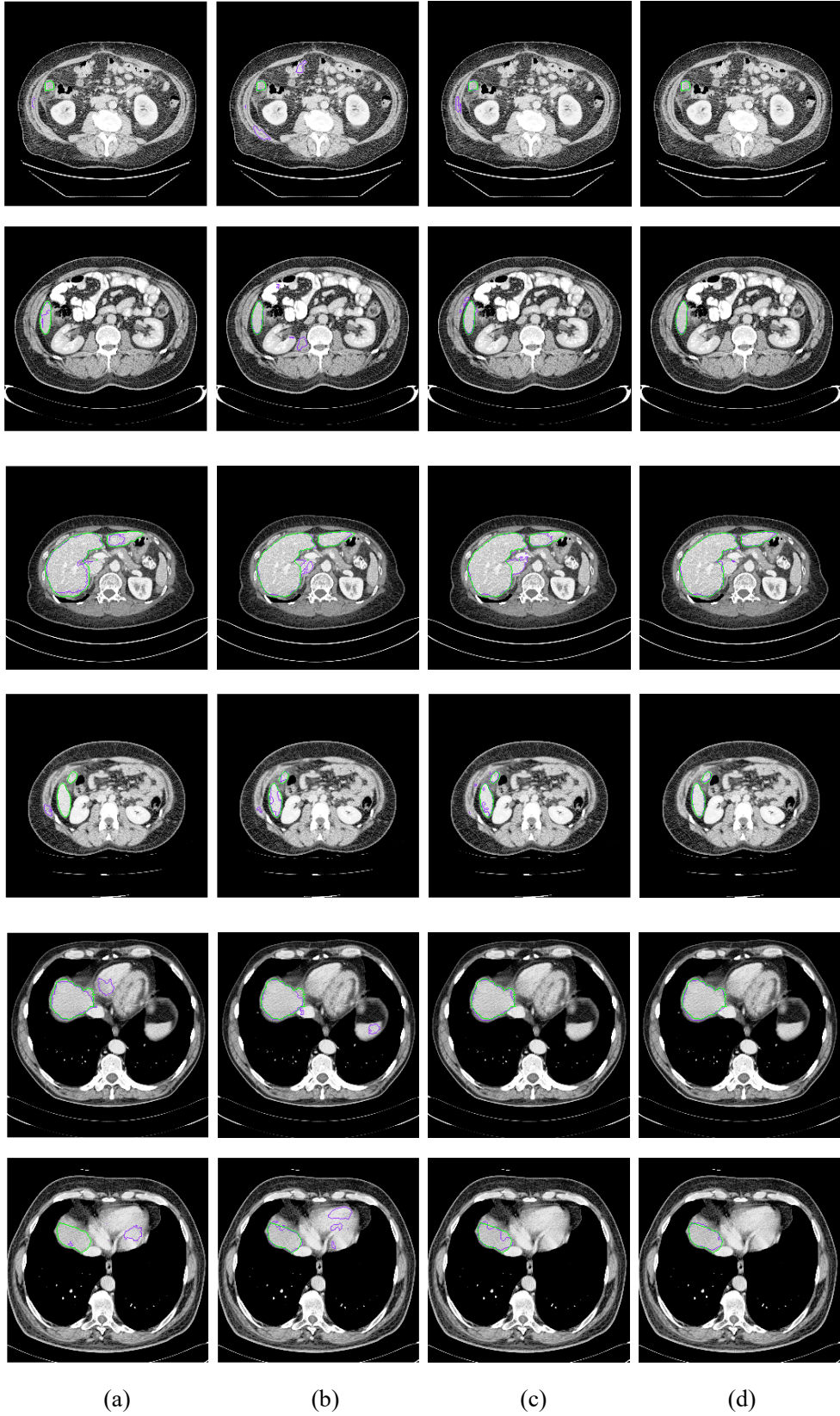


Figure 7. Comparison of the difficult segmentation problems of the four algorithms. (The first and second rows of images show small liver areas, the third and fourth rows show discontinuous areas of the liver, and the fifth and sixth rows show blurred areas of liver boundaries), where green represents the gold standard, and purple represents the results of different methods. (a) FCN (b) U-Net (c) Attention U-Net (d) Ours

Therefore, our proposed model shows relatively high robustness when dealing with difficult segmentation problems such as small liver regions, discontinuous liver areas, and blurred liver boundaries. The main reason is as following, firstly, the attention mechanism is introduced in the encoder, so that the network can pay more attention to the specific features of liver segmentation. Secondly, the atrous spatial convolutional pooling pyramid layer is utilized to extract multi-scale feature information, which effectively compensates for the loss of important combination information. Lastly, the addition of the residual structure enables the derivation of more complex image features.

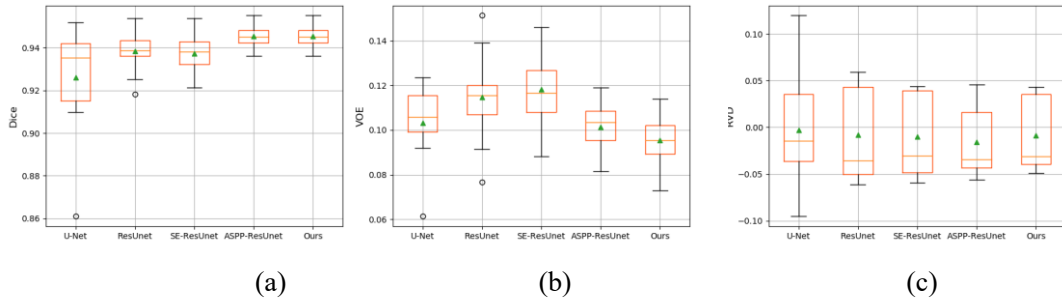
4.5 Ablation analysis on LiTS17-Training datasets

To verify the optimality of the proposed network configuration, five comparative ablation experiments were performed. Take U-Net as the baseline and make changes one by one for testing the contribution of the improved module to the overall framework. First, all convolution units in the U-Net encoder and the decoder parts are replaced with residual structures (ResU-Net). Then, the attention mechanism (SE-ResU-Net) is introduced on the basis of the ResU-Net model, which followed the convolution operation of the encoder. At last, on the basis of ResU-Net, the transition layer connecting the encoder and the decoder and the output layer of the decoder are replaced with ASPP modules. All of the models are trained and evaluated on the LiTS17 dataset. From the box plots in **Table 4** and **Figure 8**, it can be seen that, comparing to a single utilization, the combination of SE and ASPP mechanism significantly improved the performance of the U-Net-based model.

Table 4. Quantitative analysis results of ablation experiments

Model	Dice (%)	VOE (%)	RVD (%)	ASD (mm)	MSD (mm)
U-Net	92.60±2.54*	10.33±1.69	-0.28±6.13	2.41±0.54*	33.69±1.89
ResU-Net	93.85±1.04*	11.47±2.02	-0.78±4.88	1.94±0.47*	32.73±1.94
SE-ResU-Net	93.71±0.98*	11.81±1.73	-1.02±4.22	1.85±0.45*	31.05±1.56
ASPP-ResU-Net	94.20±0.51*	10.12±1.10	-1.54±3.68	1.67±0.34*	30.70±2.35
Ours	95.71±0.55	9.52±1.11	-0.84±3.86	1.54±0.30	29.14±2.63

Results are represented as mean and standard deviation. Note: * indicates a statistically significant difference between the marked result and the corresponding one of our method at a significance level of 0:05.



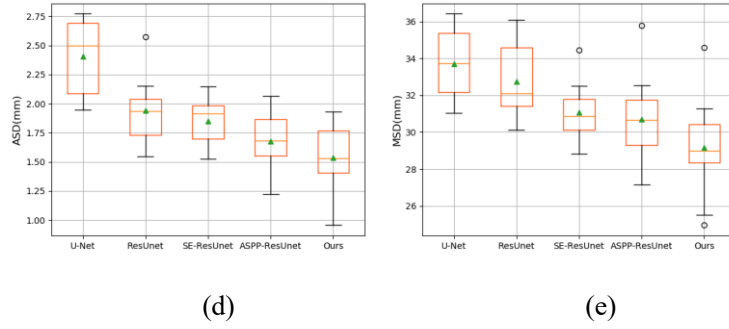


Figure 8. Comparative liver segmentation results (a) Dice (b)VOE (c) RVD (d) ASD (e) MSD

4.6 Test on Sliver07-Training dataset

To further verify the generalization ability of the proposed method, a comparative experiment was conducted using FCN, U-Net, Attention U-Net and our proposed model on 20 SLiver07-Training datasets. Table 5 and Figure 9 shows the quantitative comparative results among our method and the other three methods. It can be seen from Table 5 and Figure 9 that, compared with other five methods, our proposed method achieved the highest *Dice* of 97.31 ± 1.49 , which further proves the robustness of our method, with a detailed performance of all the metrics shown in Table 6.

Table 5. Quantitative comparison with three state-of-the-arts methods on 20 Sliver07-Training datasets

Methods	Dice (%)	VOE (%)	RVD (%)	ASD (mm)	MSD (mm)
FCN[15]	95.60±3.41*	8.23±5.89	-2.38±2.16	2.19±0.38	36.69±1.45
U-Net[16]	96.94±1.78*	5.31±3.48	-0.54±2.24	1.95±0.34	30.66±2.03
Attention U-Net[28]	96.66±2.19*	6.38±3.93	-1.29±3.58	1.80±0.38	28.30±2.05
Ours	97.31±1.49	5.37±3.27	-1.08±2.06	1.85±0.30	27.45±1.89

Results are represented as mean and standard deviation. Note: * indicates a statistically significant difference between the marked result and the corresponding one of our method at a significance level of 0:05.

Table 6. Result of our proposed SAR-U-Net on 20 SLiver07-Training datasets

Test case	Dice	VOE	RVD	ASD (mm)	MSD (mm)
1	0.945	0.103	-0.059	1.783	27.935
2	0.952	0.091	-0.067	2.284	36.534
3	0.975	0.048	-0.024	2.138	27.365
4	0.978	0.042	-0.001	1.538	25.934
5	0.934	0.156	0.011	1.959	29.446
6	0.977	0.043	-0.001	1.798	24.551
7	0.979	0.040	-0.013	2.139	30.316
8	0.974	0.050	-0.023	2.502	25.233
9	0.982	0.035	-0.011	1.618	27.428
10	0.946	0.101	0.010	2.058	26.452
11	0.985	0.029	-0.005	1.973	31.563
12	0.984	0.031	0.009	1.470	26.521
13	0.972	0.054	0.001	1.387	27.078

14	0.973	0.051	-0.020	2.059	28.726
15	0.985	0.028	0.005	2.107	25.459
16	0.984	0.031	-0.003	1.474	24.234
17	0.980	0.037	0.001	1.841	29.643
18	0.981	0.036	-0.003	1.759	28.694
19	0.988	0.024	0.003	1.636	28.419
20	0.979	0.041	-0.025	1.469	27.486
Avg	0.973	0.054	-0.0108	1.849	27.449

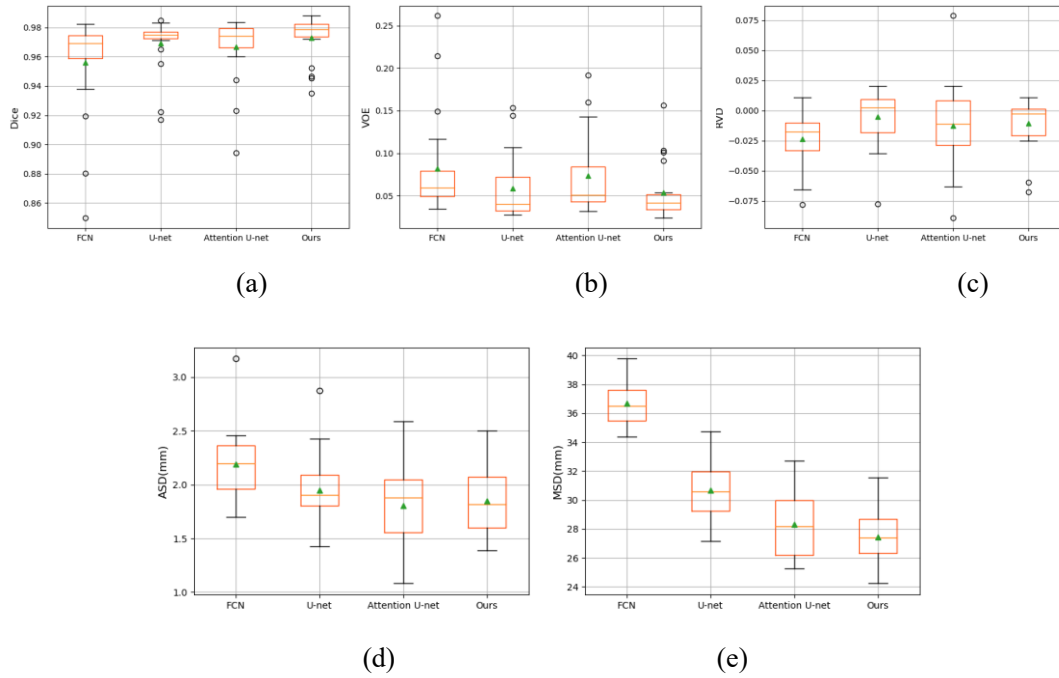


Figure 9. Comparative liver segmentation results. (a) Dice (b)VOE (c) RVD (d) ASD (e) MSD

Figure 10 shows the comparative results of 2D visualization among FCN, U-Net, Attention U-Net and our proposed method. It can be seen that, for small liver regions, discontinuous liver regions and fuzzy liver boundaries, our proposed method shows high robustness in handling these challenging segmentation cases.

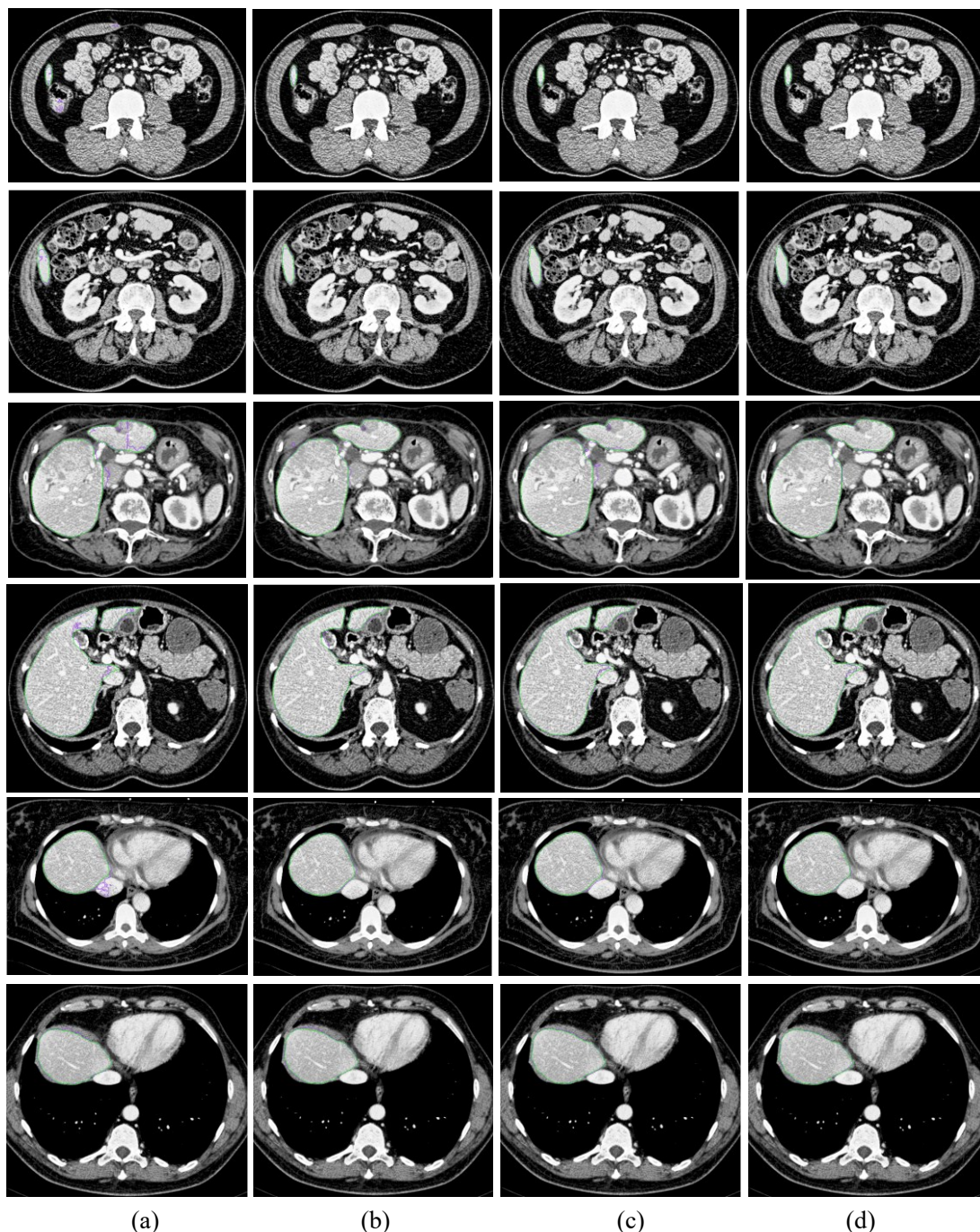


Figure 10. Test on difficult cases of SLiver07. The first and second rows denote the small liver area, the third and fourth rows denote the discontinuous liver area, and the fifth and sixth rows denote the blurred liver boundary, where the green line represents the gold standard, and the purple line represents the result of our proposed method. (a) FCN (b) U-Net (c) Attention U-Net (d) Ours

4.7 Limitations

Although encouraging results were obtained by our proposed SAR-U-Net framework, limitations still exist for further enhancement. Our proposed method is based on 2D network, but the CT images are 3D-based, thus it is prone to miss important context information on the z-axis. In addition, once the liver edge contains lesions or tumor abnormalities (as shown in **Figure 11**), the proposed method may result in large

errors around the boundary. Regarding such limitations, evolving the current 2D framework to 3D would further improve the accuracy via context of z-axis, and thus reduce the errors around the liver abnormalities.

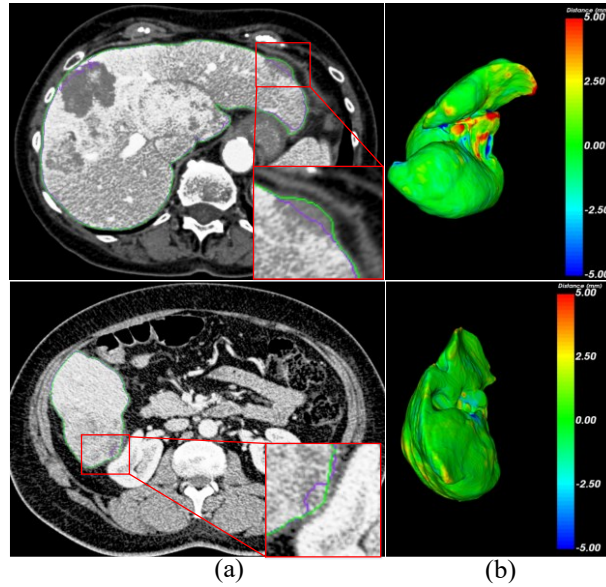


Figure 11. Limitations on liver boundary lesions of proposed method. (a) 2D error visualization (the green line indicates the gold standard, while the purple line indicates our results) (b) 3D error visualization (Blue and red indicate large over-segmentation and under-segmentation errors, while green indicates small errors.)

5 Conclusion

This paper proposes a novel SAR-U-Net network for automatic liver segmentation from CT. The U-Net based framework leverages the advantages of Squeeze-and-Excitation, Atrous Spatial Pyramid Pooling and residual learning techniques. First, the SE-based attention mechanism is used to derive image features in an adaptive manner, and irrelevant areas are suppressed, so that the network focuses on the relevant characteristics of the liver segmentation task; Then, the ASPP technique is used as the transition and output layers the network, to achieve the multi-scale extraction of the feature image. Furthermore, the residual structure is added into the convolution unit to handle the degradation problem.

The high accuracy and robustness of our proposed model were verified on two competition training datasets, LiTS17 and SLiver07. Compared with the related classic methods, our method showed superior performance on the quantitative metrics. Specifically, the proposed method showed a significant improvement and robustness in handling small liver regions, discontinuous liver regions and blurry liver boundaries. Nevertheless, our proposed method is prone to slight over-segmentation or under-segmentation errors, when dealing with lesions or tumors around liver boundary, and thus make full use of the z-axis information in 3D to reduce errors would be the focus of our future work.

Conflict of Interest

The authors declare there is no conflict of interest in this study.

Reference

- [1] L. Soler, H. Delingette, G. Malandain, J. Montagnat, N. Ayache, C. Koehl, O. Dourthe, B. Malassagne, M. Smith, D. Mutter et al., “Fully automatic anatomical, pathological, and functional segmentation from ct scans for hepatic surgery,” *Computer Aided Surgery*, vol. 6, no. 3, pp. 131–142, 2001.
- [2] J. H. Moltz, L. Bornemann, V. Dicken, and H. Peitgen, “Segmentation of liver metastases in ct scans by adaptive thresholding and morphological processing,” in *MICCAI workshop*, vol. 41, no. 43, 2008, p. 195.
- [3] X. Lu, J. Wu, and X. Ren, “The study and application of the improved region growing algorithm for liver segmentation,” *Optik - International Journal for Light and Electron Optics*, vol. 125, pp. 2142–2147, September 2014.
- [4] S. D. S. Alshaikhli, M. Y. Yang, and B. Rosenhahn, “Automatic 3D liver segmentation using sparse representation of global and local image information via level set formulation,” *Computer Science*, 2015.
- [5] J. Lee, N. Kim, H. Lee, J. B. Seo, H. J. Won, Y. M. Shin, Y. G. Shin, and S.-H. Kim, “Efficient liver segmentation using a level-set method with optimal detection of the initial liver boundary from level-set speed images,” *Computer Methods and Programs in Biomedicine*, vol. 88, no. 1, pp. 26–38, 2007.
- [6] Häme. Y, “Liver Tumor Segmentation Using Implicit Surface Evolution,” *Proceedings of the MICCAI Workshop on 3D Segmentation in the Clinic: A Grand Challenge II 2008*.
- [7] Massoptier. L, and Casciaro. S, “A New Fully Automatic and Robust Algorithm for Fast Segmentation of Liver Tissue,” *European Radiology*, vol.18, Issue.8, 2008, pp.1658-1665.
- [8] J.S. Jin, and S.K. Chalup, “A Liver Segmentation Algorithm Based on Wavelets and Machine Learning,” *International Conference on Computational Intelligence and Natural Computing*, 2009, pp. 122–125.
- [9] X. Li, C. Huang, and F. Jia, “Automatic Liver Segmentation Using Statistical Prior Models and Free-form Deformation,” *International MICCAI Workshop on Medical Computer Vision*, Springer, Cham, vol. 8848, 2014, pp. 181–188.
- [10] Shi C, Cheng Y, Wang J, et al. Low-rank and sparse decomposition based shape model and probabilistic atlas for automatic pathological organ segmentation[J]. *Medical image analysis*, 2017, 38: 30-49.
- [11] Wang J, Cheng Y, Guo C, et al. Shape–intensity prior level set combining probabilistic atlas and probability map constrains for automatic liver segmentation from abdominal CT images[J]. *International journal of computer assisted radiology and surgery*, 2016, 11(5): 817-826.
- [12] Krizhevsky A, Sutskever I, Hinton G E. Imagenet classification with deep convolutional neural networks[C]//Advances in neural information processing systems. 2012: 1097-1105.
- [13] He K, Zhang X, Ren S, et al. Deep residual learning for image recognition[C]//Proceedings of the IEEE conference on computer vision and pattern recognition. 2016: 770-778.
- [14] Ren S, He K, Girshick R, et al. Faster r-cnn: Towards real-time object detection with region proposal networks[C]//Advances in neural information processing systems. 2015: 91-99.
- [15] J. Long, E. Shelhamer, and T. Darrell, “Fully convolutional networks for semantic

- segmentation,” IEEE Conference on Computer Vision and Pattern Recognition, IEEE Computer Society, 2015, pp. 3431-3440.
- [16] O. Ronneberger, P. Fischer, and T. Brox. “U-Net: Convolutional Networks for Biomedical Image Segmentation,” International Conference on Medical Image Computing and Computer-Assisted Intervention, Springer, Cham, 2015, pp. 234–241.
- [17] F. Milletari, N. Navab, and S.-A. Ahmadi, “V-Net: Fully Convolutional Neural Networks for Volumetric Medical Image Segmentation,” in 2016 Fourth International Conference on 3D Vision, 2016, pp. 565-571.
- [18] K. He, X. Zhang, and S. Ren, “Deep Residual Learning for Image Recognition,” The IEEE Conference on Computer Vision and Pattern Recognition (CVPR), 2016, pp. 770–778.
- [19] Christ, Patrick Ferdinand, et al. "Automatic liver and lesion segmentation in CT using cascaded fully convolutional neural networks and 3D conditional random fields.", in MICCAI, 2016.
- [20] Kaluva, K.C., Khened, M., Kori, A., Krishnamurthi, G., 2018. 2d-densely connected convolution neural networks for automatic liver and tumor segmentation. arXiv preprint arXiv:1802.02182 .
- [21] Li, Xiaomeng, et al. "H-DenseU-Net: Hybrid densely connected U-Net for liver and liver tumor segmentation from CT volumes.", in arXiv preprint arXiv:1709.07330, 2017.
- [22] Han X. Automatic liver lesion segmentation using a deep convolutional neural network method[J]. arXiv preprint arXiv:1704.07239, 2017.
- [23] F. Wang, M. Jiang, C. Qian, S. Yang, C. Li, H. Zhang, X. Wang, and X. Tang, “Residual Attention Network for Image Classification,” in IEEE Conference on Computer Vision and Pattern Recognition, 2017, pp. 6450–6458.
- [24] L. C. Chen, Y. Yang, J. Wang, W. Xu, and A. L. Yuille, “Attention to scale: Scale-aware semantic image segmentation,” in IEEE Conference on Computer Vision and Pattern Recognition, 2016, pp. 3640–3649.
- [25] Y. Zhu, C. Zhao, H. Guo, J. Wang, X. Zhao, and H. Lu, “Attention CoupleNet: Fully convolutional attention coupling network for object detection,” IEEE Trans. Image Process., vol. 28, no. 1, pp. 113–126, Jan. 2018.
- [26] B. Zhao, X. Wu, J. Feng, Q. Peng, and S. Yan, “Diversified visual attention networks for fine-grained object classification,” IEEE Trans. Multimedia, vol. 19, no. 6, pp. 1245–1256, Jun. 2017
- [27] J. Hu, L. Shen, and G. Sun, “Squeeze-and-excitation networks,” in Proceedings of IEEE conference on computer vision and pattern recognition (CVPR), 2018, pp. 7132–7141.
- [28] O. Oktay et al. (2018). “Attention U-Net: Learning where to look for the pancreas.” [Online]. Available: <https://arxiv.org/abs/1804.03999>.
- [29] J. Schlemper, O. Oktay, L. Chen, J. Matthew, C. Knight, B. Kainz, B. Glocker, and D. Rueckert, “Attention-Gated Networks for Improving Ultrasound Scan Plane Detection,” arXiv preprint arXiv:1804.05338, 2018
- [30] Chen LC, Papandreou G, Kokkinos I et al (2017) DeepLab: semantic image segmentation with deep convolutional nets, atrous convolution, and fully connected CRFs. IEEE Trans Pattern Anal Mach Intell 40(4):834–848.
- [31] Simard P Y, Steinkraus D, Platt J C. Best practices for convolutional neural networks applied to visual document analysis[C]//Icdar. 2003, 3(2003).
- [32] F. Yu and V. Koltun, "Multi-scale context aggregation by dilated convolutions," arXiv preprint

arXiv:1511.07122, 2015.

- [33] Chen L C, Papandreou G, Kokkinos I et al (2014) Semantic image segmentation with deep convolutional nets and fully connected CRFs. *Comput Sci* 4:357–361.
- [34] Jin Q, Meng Z, Sun C, Cui H, Su R. “RA-U-Net: A Hybrid Deep Attention-Aware Network to Extract Liver and Tumor in CT Scans,” arXiv preprint arXiv:1811.01328, 2018.
- [35] L. Bi, J. Kim, A. Kumar, and D. Feng, “Automatic Liver Lesion Detection using Cascaded Deep Residual Networks,” arXiv preprint arXiv:1704.02703, 2017.
- [36] Noori, Mehrdad, Ali Bahri, and Karim Mohammadi. "Attention-guided version of 2D U-Net for automatic brain tumor segmentation." 2019 9th International Conference on Computer and Knowledge Engineering (ICCKE). IEEE, 2019.